Isotactic Polypropylene/Polymethylmethacrylate Blends: Effects of Addition of Propylene-*Graft*-Methylmethacrylate Copolymer

L. D'ORAZIO,[1] R. GUARINO,[1] C. MANCARELLA,[1] E. MARTUSCELLI,[1] G. CECCHIN[2]

[1] Istituto di Ricerca e Tecnologia delle Materie Plastiche del CNR Via Toiano, 6-80072 Arco Felice, Napoli, Italy

[2] Montell, Ferrara, Italy

Received 22 November 1996; accepted 24 January 1997

ABSTRACT: A novel graft copolymer of unsaturated propylene with methyl methacrylate (uPP-*g*-PMMA) was added to binary blends of isotactic polypropylene (iPP) and atactic poly(methyl methacrylate) (aPMMA) with a view to using such a copolymer as a compatibilizer for iPP/aPMMA materials. Optical microscopy (OM), scanning electron microscopy, wide angle X-ray scattering (WAXS), and small angle X-ray scattering (SAXS) techniques showed that, contrary to expectation, the uPP-*g*-PMMA addition does not provide iPP/aPMMA compatibilized materials, irrespective of composition. As a matter of fact the degree of dispersion of the minor component achieved following the addition of uPP-*g*-PMMA copolymer remained quite comparable to that exhibited by binary blends of iPP and aPMMA with no relevant evidence of adhesion or interconnection between the phases. On the other hand the crystalline texture was deeply modified by the copolymer presence. With increasing uPP-*g*-PMMA content (w/w) the iPP spherulites were found to become more open and coarse and the dimensions and number per unit area of the amorphous interspherulitic contact regions were found to increase. According to such OM results the copolymer uncrystallizable sequences were assumed to be mainly located in interfibrillar and interspherulitic amorphous contact regions. SAXS analysis demonstrated that the phase structure developed in the iPP/aPMMA/uPP-*g*-PMMA blends is characterized by values of the long period increasing linearly with increasing copolymer content (w/w). Assuming a two phase model for the iPP spherulite fibrillae, constituted of alternating parallel crystalline lamellae and amorphous layers, the lamellar structure of the iPP phase in the ternary blends is characterized by crystalline lamellar thickness (L_c) and an interlamellar amorphous layer (L_a) higher than that shown by plain iPP and L_c and L_a values both increased with increasing uPP-*g*-PMMA content (w/w). Such SAXS results have been accounted for by assuming that a cocrystallization phenomenon between propylenic sequences of the uPP-*g*-PMMA copolymer and iPP occurs. The development of the iPP lamellar structure in the iPP/aPMMA/uPP-*g*-PMMA blends was thus modeled hypothesizing that during such a cocrystallization process copolymer PMMA chains with comparatively lower molecular mass remain entrapped into the iPP interlamellar amorphous layer forming their own domains. Moreover, evidence of strong correlations between the crystallization process of the uPP-*g*-PMMA copolymer and the iPP crystallization process was shown also by differential scanning calorimetry and WAXS experiments.
 J Appl Polym Sci **66:** 2377–2393, 1997

Key words: novel graft copolymer; compatibilizer; unsaturated propylene; methyl methacrylate; isotactic polypropylene; atactic poly(methyl methacrylate)

Correspondence to: Dr. L. D'Orazio.

Journal of Applied Polymer Science, Vol. 66, 2377–2393 (1997)
 CCC 0021-8995/97/132377-17

INTRODUCTION

It is well known that isotactic polypropylene (iPP), owing to its saturated hydrocarbon structure, cannot be used for applications where reactivity or polarity are required. To open new opportunities for iPP based materials in such fields, one approach involves addition of compatibilizers as third components to binary blends constituted by iPP and polar polymer or iPP and reactive polymer. In a previous article[1] we reported on the results of investigations to compatibilize iPP/atactic polystyrene (aPS) blends by addition of an unsaturated butadiene/propylene copolymer (uPP) that had been grafted with aPS (uPP-*g*-PS). Such a molecule, in which the butadiene is linked mainly in the 1,2 configuration, had been synthetized "*ad hoc*" according to the procedure patented by Cecchin et al.[2,3] from Himont. Our previous study[1] showed that the addition of uPP-*g*-PS copolymer can provide iPP/aPS compatibilized materials and that the extent of the compatibilization achieved is composition dependent. Depending on copolymer content (w/w) the type of interface generated in the blend materials can be modeled according to a core shell or to an interfacial interpenetration model. Furthermore, it has been demonstrated[1] that in the uPP-*g*-PS copolymer there are propylenic sequences that are able to crystallize in the α form of PP and that the crystallization processes of the iPP and uPP-*g*-PS copolymer are strongly correlated. Assuming for the iPP spherulites fibrillae a two phase model constituted by alternating parallel crystalline lamellae and amorphous layers, small angle X-ray scattering (SAXS) investigations revealed that in uPP-*g*-PS both the thickness of crystalline lamellae (L_c) and that of the amorphous layers (L_a) are greater than those measured for iPP; the L_a increases rapidly with increasing copolymer content. In line with the SAXS results the development of the lamellar structure of the iPP phase was modeled assuming that propylenic sequences of the uPP-*g*-PS copolymer cocrystallize with iPP; during such a process aPS chains grafted into copolymer sequences remain entrapped in iPP interlamellar amorphous layers where they form separated domains.

In the present article we report on the results of investigations regarding the effects of the addition of a graft copolymer of propylene with methyl methacrylate (uPP-*g*-PMMA) to binary iPP/atactic poly(methyl methacrylate) (aPMMA) blends. Also such an uPP-*g*-PMMA copolymer was synthetized *ad hoc* by grafting PMMA via metallation along the backbone chain of the same sample of uPP used to obtain the uPP-*g*-PS copolymer. Both the uPP metallation reaction and subsequent modification with anionic polymerization of the MMA monomer were conducted in the same way as for styrene.[3] The main aim of this study is to assess if the uPP-*g*-PMMA copolymer is suitable for compatibilizing PP with PMMA or with homopolymers miscible with PMMA. Molecular, structural, morphological, and thermal characterization of the uPP-*g*-PMMA copolymer was already reported.[4] This study shows that the PMMA phase is present in long blocks with a few points of insertion, the PMMA being atactic. Moreover, it was demonstrated that in the uPP-*g*-PMMA copolymer there are propylenic sequences able to crystallize in the α form of iPP. The value of the equilibrium melting temperature (T_m) of such sequences was calculated according to the kinetic theory of polymer crystallization and was found to be in good agreement with the T_m value obtained by plotting the apparent melting temperature versus the inverse of lamellar thickness by SAXS. Results were about 30 K lower than that reported for iPP, indicating the presence of defects in the uPP-*g*-PMMA crystals. A free energy of folding value much lower than that reported in the literature for iPP confirmed a very irregular and perturbed surface of such crystals. Dynamic mechanical thermal analysis (DMTA), differential scanning calorimetry (DSC), optical microscopy (OM), scanning electron microscopy (SEM), and wide and small angle X-ray scattering (WAXS and SAXS) were therefore used to investigate the morphology and structure of phases and interphases developed in iPP/aPMMA/uPP-*g*-PMMA blends containing 2, 5, and 10% (w/w) of uPP-*g*-PMMA copolymer in samples obtained by solution casting. This work, as well as the previous,[1,4] was undertaken in the framework of our research on iPP based blends.[5–10]

EXPERIMENTAL

Materials

The starting polymers used in this study were iPP (HS005) made by Himont, an aPMMA made by

Table I Molecular Characteristics of Starting iPP and uPP-*g*-PMMA Copolymer and with Glass Transition Temperature (T_g), Apparent Melting Temperature (T'_m), and Crystallinity Index (X_c)

Sample	$\bar{M}_n$ (g/mol)	$\bar{M}_w$ (g/mol)	$\bar{M}_w/\bar{M}_n$	η (d/g)	% PMMA (w/w)	T_g (°C)	T'_m (°C)	X_c
iPP	78,700	509,000	6.5	2.0	—	7	165	0.55
uPP-*g*-PMMA	—	—	—	1.3	20	23	129 141	0.28

BDH Chemicals Ltd. (U.K.), and an uPP-*g*-PMMA copolymer synthesized in the Himont Scientific Laboratories according to methods patented by Cecchin et al.[2,3] from Himont. The aPMMA sample has a weight average molecular mass (M_w) equal to 116,000 and a glass transition temperature (T_g) of 134°C; the molecular characteristics of the iPP and uPP-*g*-PMMA samples are reported in Table I.

Blending and Sample Preparation

All the investigated samples were obtained by means of the solvent casting method. The blend components were dissolved in a common solvent, *o*-dichlorobenzene, at a total polymer concentration of 3% by weight and at a temperature of 135°C. Thin films were then obtained by *o*-dichlorobenzene casting carried out under a vacuum at 135°C for 3 h. iPP/aPMMA (80/20 w/w) binary blends and iPP/aPMMA/uPP-*g*-PMMA ternary blends containing 2, 5, and 10% (w/w) of graft copolymer were prepared.

Techniques

DSC

The thermal behavior of the thin films of plain starting components and blends obtained by casting was analyzed by means of DSC with a Mettler TA 3000 instrument equipped with a control and programming unit (microprocessor Tc 10). The apparent melting temperatures (T'_m) and the crystallinity index (X_c) were determined following this procedure: the samples (about 9 mg) were heated from room temperature up to 215°C at a rate of 10°C/min and the heat evolved during the scanning process was recorded as a function of temperature. The observed melting temperatures (T'_m) and the apparent enthalpies of melting (ΔH^*) were obtained from the maxima and the area of the melting peaks, respectively. The crystallinity index (X_c) of the iPP and the blends were calculated by applying the following relations:

$$X_c(\text{iPP}) = \Delta H^*(\text{iPP})/\Delta H^0(\text{iPP}) \quad (1)$$

$$X_c(\text{blend}) = \Delta H^*(\text{blend})/\Delta H^0(\text{iPP}) \quad (2)$$

where ΔH^*(iPP) is the apparent enthalpy of fusion per gram of iPP in the blend; ΔH^0(iPP) is the heat of fusion per gram of 100% crystalline iPP, [ΔH^0(iPP) = 209 J/g][11]; and ΔH^*(blend) is the apparent enthalpy of fusion per gram of blend. The crystalline weight fractions referred to the iPP phase in the blends [X_c(iPP)] were calculated from the following relation:

$$X_c(\text{iPP}) = X_c(\text{blend})/W(\text{iPP}) \quad (3)$$

where W(iPP) is the weight fraction of iPP in the blends.

The effect of the nucleating ability of PMMA and uPP-*g*-PMMA copolymer on the crystallization process of iPP was investigated following this procedure: the samples were heated up to 215°C at a rate of 10°C/min and were kept at this temperature for 10 min to destroy any traces of crystallinity and then cooled at a rate of 10°C/min.

DMTA

The tangent δ and storage modulus of all investigated samples were measured by means of DMTA (Rheometric Scientific MK III). Test data were collected in tensile mode from −40 to 140°C using a scanning rate of 1.5°C/min and a frequency of 1 Hz.

OM

The thin films of plain starting components and blends as obtained from solution casting were observed by means of OM. A Leitz optical polarizing microscope fitted with a Mettler hot stage was used;

optical micrographs were taken with crossed and parallel polarizers.

SEM

Cryogenically fractured surfaces of thin films of binary and ternary blends were observed by means of a Philips XL 20 scanning electron microscope after coating with gold-palladium.

WAXS

WAXS studies were carried out by means of a PW 1060/71 Phillips diffractometer (Cu Kα Ni-filtered radiation) equipped with a sample carrier for sample spinning; the high voltage was 40 kV and the tube current was 30 mA. A standard sample was employed to determine the instrumental broadening.

SAXS

SAXS studies were carried out by means of a compact Kratky camera equipped with a Braun 1-dimensional positional sensitive detector. Ni-filtered Cu Kα radiation generated from a Phillips X-ray generator (PW 1730/10) operating at 40 kV and 30 mA, was used. The raw scattering data were corrected for parasitic scattering, absorption, and slit smearing by using Vonk's method.[12] The desmeared intensities were then Lorentz factor corrected by multiplying by s^2 ($s = 2 \sin \theta/\lambda$).[13]

RESULTS AND DISCUSSION

Thermal Behavior

The variation of tangent δ with temperature obtained for the binary iPP/aPMMA shows that such a system possesses individual glass transition temperatures of the single components, as expected for an immiscible polymer blend. By adding uPP-*g*-PMMA copolymer, irrespective of blend composition, no significant shift in the T_g values attributed to the iPP phase is observed. On the other hand the T_g value attributed to the PMMA phase is slightly higher than that found in the iPP/aPMMA binary blends (see Table II). Such a result could suggest a comparatively lower molecular mobility of the PMMA phase in the ternary blends. As for the plain uPP-*g*-PMMA copolymer, DMTA measurements show that such a copolymer exhibits two distinct T_g values: the first one located at 23°C was attributed to propylenic sequences, and the second one at a temperature higher than 100°C was attributed to the PMMA phase. Unfortunately such a T_g value cannot be detected precisely owing to sample softening during the test and they also are undetectable by DSC experiments. It is interesting that the copolymer transition located at 23°C is no longer observed in the ternary blends, irrespective of the uPP-*g*-PMMA content (w/w) because a single T_g is found for the iPP phase. Such a finding could suggest that the T_g of the uPP-*g*-PMMA propylenic sequences up to the iPP T_g is shifted by the occurrence of favorable intermolecular interactions between the copolymer propylenic sequences and iPP (i.e., by miscibility effects in the amorphous condensed state).

The DSC thermograms of the binary iPP/aPMMA and ternary iPP/aPMMA/uPP-*g*-PMMA blends show a single endothermic peak when heated from room temperature up to 200°C. It is noted that such a peak widens by uPP-*g*-PMMA addition and that the extent of such an effect is composition dependent; the observed broadening in fact increases on increasing the uPP-*g*-PMMA content (see Fig. 1). The temperatures corresponding to the maxima of such peaks (T'_m) are reported in Table II together with the crystallinity index of the blends [X_c(blend)] and the iPP phase [X_c(iPP)]. From such data it emerges that the T'_m and [X_c(blend)] values are almost independent of blend composition and are quite comparable to that shown by the plain iPP. As for the [X_c(iPP)] values, the iPP phase crystallized from its ternary blends shows crystallinity indices lower than that exhibited by the iPP phase crystallized from the binary iPP/aPMMA blend with no composition dependence (see Table II). Such a result, together with the finding that crystals grown in the presence of the uPP-*g*-PMMA phase show perfection decreasing* and/or size distribution widening with higher copolymer content in the blend (see Fig. 1), suggests that the uPP-*g*-PMMA interferes with the iPP crystallization process. The DSC thermogram of the plain uPP-*g*-PMMA copolymer shows a double melting peak, the lower temperature component being broader and of lower intensity than the higher temperature component (see Fig. 2). The temperatures of both peaks are reported in Table I and are considerably lower than that shown by the iPP phase. Taking into account that, irrespective of copolymer content in the blend, no separate melting of the uPP-*g*-PMMA propylenic sequences is de-

*See the explanation.

Table II Glass Transition Temperature (T_g), Apparent Melting Temperature (T'_m), Crystallinity Index of Binary iPP/aPMMA, and Ternary iPP/aPMMA/uPP-*g*-PMMA Ternary Blends [X_c (Blend)] and Crystallinity Index of iPP Phase [X_c (iPP)]

Sample	T_g (°C)	T'_m (°C)	X_c	
			Blend	iPP
iPP/aPMMA	12 130	167	0.42	0.53
iPP/aPMMA/uPP-*g*-PMMA graft 2% (w/w)	13 133	165	0.41	0.51
iPP/aPMMA/uPP-*g*-PMMA graft 5% (w/w)	14 135	166	0.42	0.53
iPP/aPMMA/uPP-*g*-PMMA graft 10% (w/w)	12 134	165	0.41	0.51

tected, it could be hypothesized that such sequences are able to cocrystallize and the iPP allows the formation of crystalline phases with different *perfection and/or thickness. Analogous results were obtained while studying the effects of the addition of uPP-*g*-PS copolymer on the crystallization process of iPP/atactic PS blends.[1]

The DSC nonisothermal crystallization exotherms from the melt of the plain iPP is compared in Figure 3 with those shown by the iPP phase that were nonisothermally crystallized from melts of the binary iPP/aPMMA and ternary iPP/aPMMA/uPP-*g*-PMMA blends. As shown, when the iPP crystallizes in the presence of PMMA and/or uPP-*g*-PMMA copolymer, the range of crystallization temperature remains comparable to that shown by the plain iPP, indicating that both PMMA and/or uPP-*g*-PMMA copolymer have no nucleating ability on the crystallization process of the iPP. Notably the uPP-*g*-PMMA copolymer shows a range of nonisothermal crystallization partially included in that shown by the plain iPP, confirming that its crystallization process from the melt is correlated with that of the plain iPP.

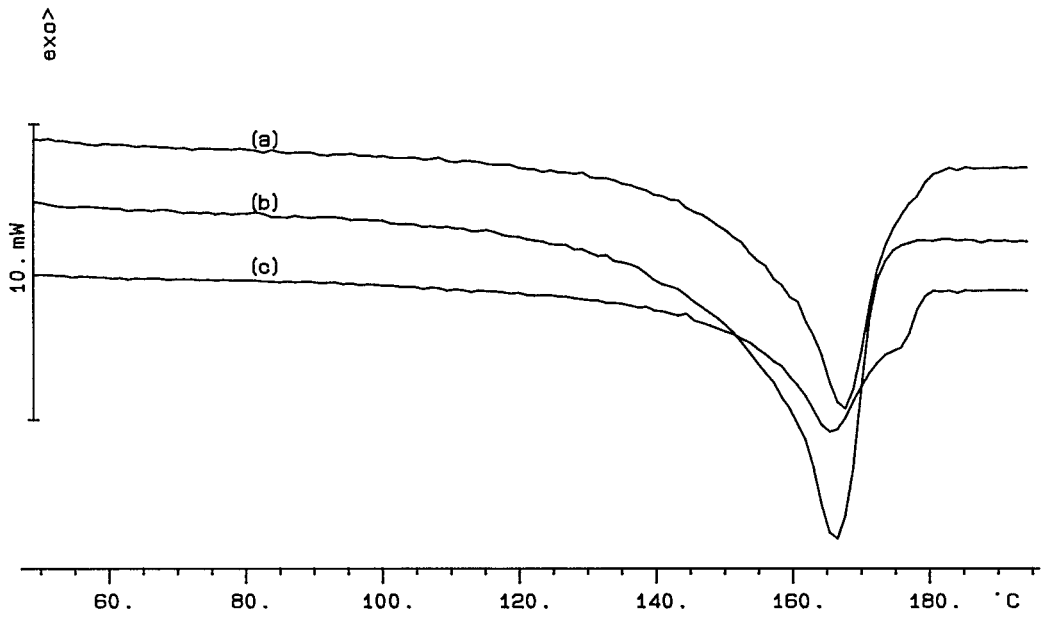

Figure 1 DSC thermograms of (a) binary iPP/aPMMA and ternary iPP/aPMMA/uPP-*g*-PMMA blends containing (b) 2% (w/w) and (c) 10% (w/w) of uPP-*g*-PMMA copolymer.

Figure 2 DSC thermogram of plain uPP-*g*-PMMA copolymer.

The DSC melting endotherms of nonisothermally crystallized samples of binary and ternary blends are shown in Figure 4; when heated from room temperature up to 200°C, a single endothermic peak is exhibited by all the investigated samples in agreement with the thermal behavior shown by the samples obtained from solution casting. The temperature positions of the maxima of the observed peaks (T'_m), X_c(blend), and X_c(iPP) values are reported in Table III; the trend of such data agrees with that found for the cast samples, even though, because of the crystallization condi-

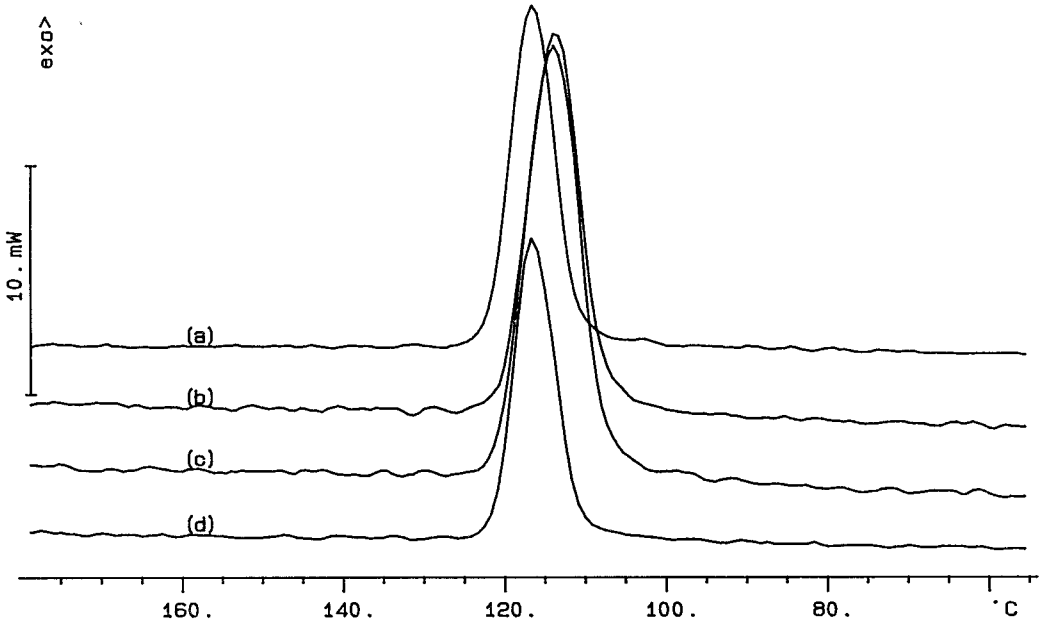

Figure 3 Nonisothermal crystallization curves for (a) plain iPP and for the iPP phase crystallized from its (b) binary iPP/aPMMA blends and ternary iPP/aPS/uPP-*g*-PMMA blends containing (c) 2% (w/w) and (d) 10% (w/w) of uPP-*g*-PMMA copolymer.

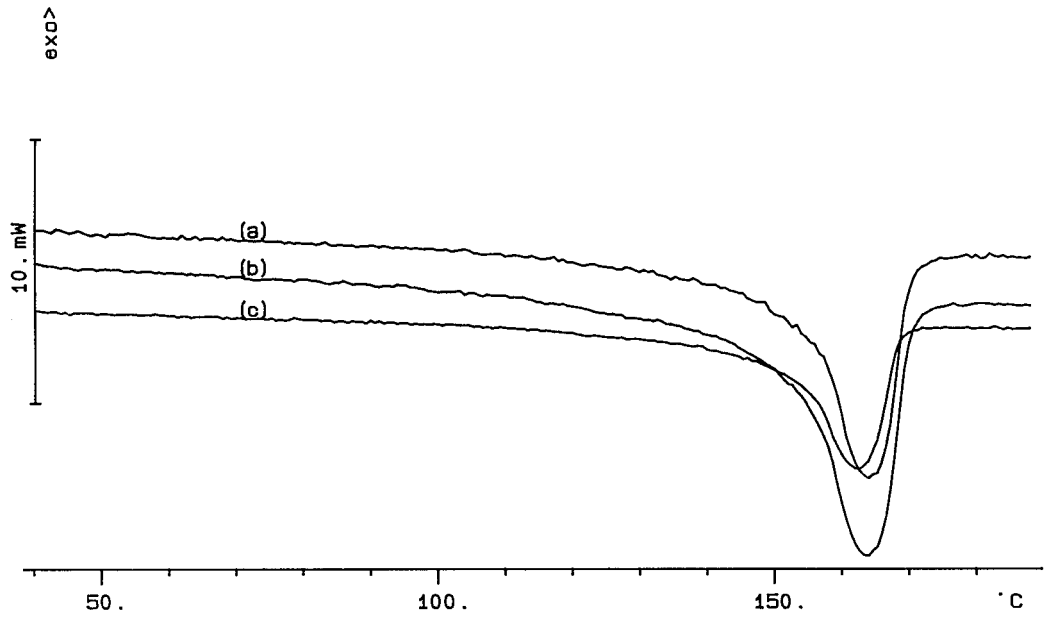

Figure 4 DSC thermograms of nonisothermally crystallized samples of (a) binary iPP/aPMMA and ternary iPP/aPMMA/uPP-*g*-PMMA blends containing (b) 2% (w/w) and (c) 10% (w/w) of uPP-*g*-PMMA copolymer.

tions imposed, such values are lower than that shown by the iPP phase in the solution cast samples (compare Tables II, III).

Phase Structure

Microscopy Studies

Figure 5 shows optical micrographs (taken at crossed and parallel polarizers) of thin films of the binary (80/20 w/w) iPP/aPMMA blends; for comparison the optical micrographs of thin films of the plain iPP and uPP-*g*-PMMA copolymer are also shown. The iPP/aPMMA blends exhibit a regular spherulitic superstructure and the PMMA phase is segregated in spherical shaped domains mainly occluded in the iPP intraspherulitic regions; furthermore, there are some amorphous interspherulitic contact regions. Amorphous interspherulitic contact regions are shown also by the plain iPP, in agreement with results obtained by

Table III Nonisothermal Crystallization Range for Plain iPP and uPP-*g*-PMMA Copolymer and iPP Nonisothermally Crystallized from Its Binary and Ternary Blends together with Apparent Melting Temperature (T'_m), Blend Crystallinity Index [X_c (Blend)] and Crystallinity Index of iPP Phase [X_c (iPP)]

Sample	Nonisothermal Crystallization Range (°C)	T'_m (°C)	X_c	
			Blend	iPP
iPP	125–99	163	0.48	0.48
iPP/aPMMA	126–95	163	0.38	0.48
iPP/aPMMA/uPP-*g*-PMMA graft 2% (w/w)	127–95	163	0.37	0.46
iPP/aPMMA/uPP-*g*-PMMA graft 5% (w/w)	125–99	162	0.35	0.44
iPP/aPMMA/uPP-*g*-PMMA graft 10% (w/w)	125–99	162	0.36	0.45
uPP-*g*-PMMA	114–80	139	0.29	0.36

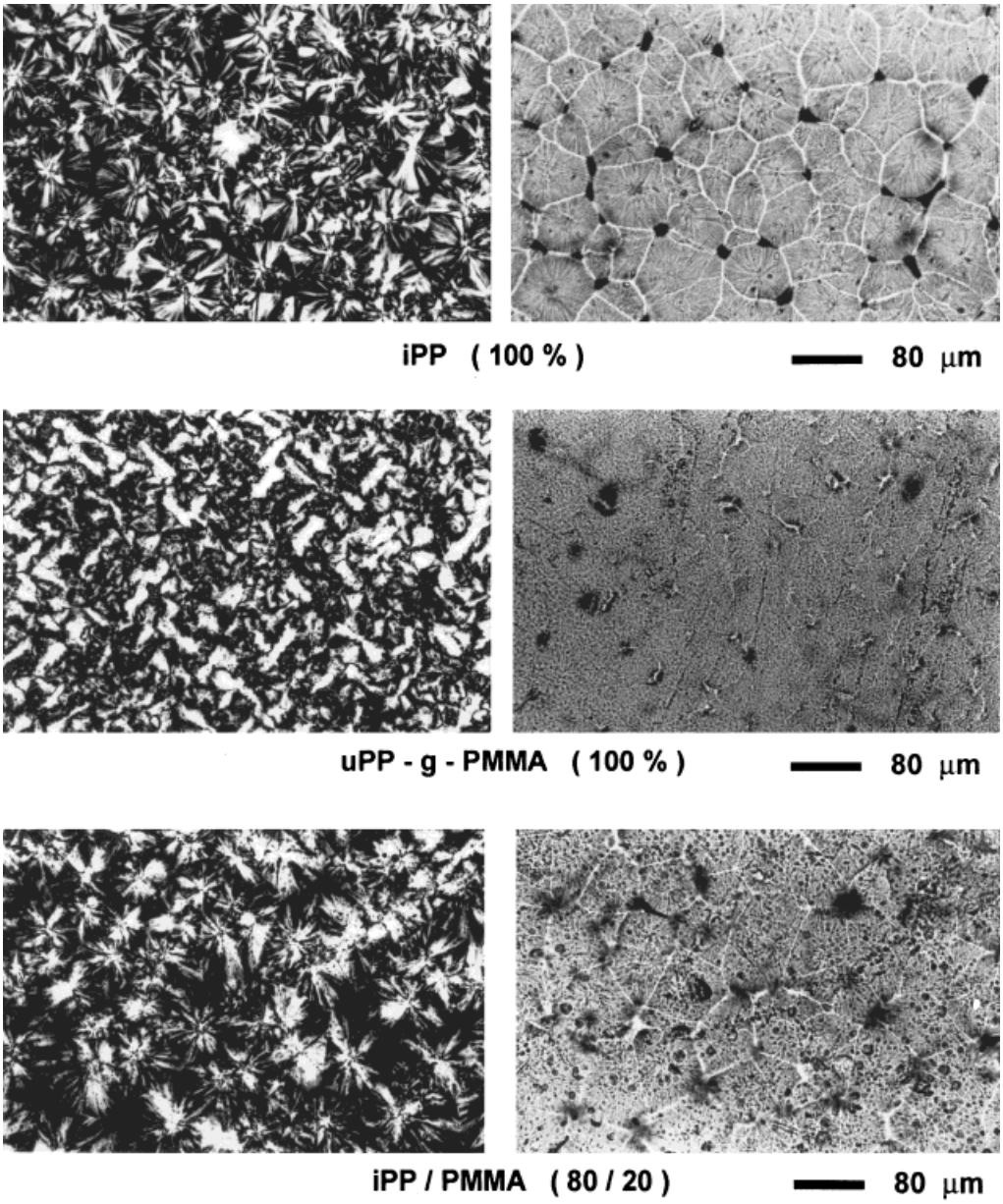

Figure 5 Optical micrographs taken with crossed and parallel polarizers of thin films of binary iPP/aPMMA blends and plain iPP and uPP-*g*-PMMA copolymer.

studying the influence of the crystallization conditions on the structure of phases and interphases developed after complete crystallization of the iPP under controlled crystallization conditions.[6] As far as the plain uPP-*g*-PMMA copolymer is concerned, the finding that a well defined spherulitic superstructure is formed agrees with results obtained while studying the phase structure of isothermally crystallized copolymer samples.[4] In addition, amorphous material is found at spherulitic boundary regions, suggesting that the growth front of the crystals tends to reject propylenic sequences with comparatively lower constitutional and configurational regularity. Crossed and parallel polarizer optical micrographs of the iPP/aPMMA/uPP-*g*-PMMA ternary blends are shown in Figure 6. For low copolymer content (2% w/w) the iPP phase crystallizes, forming spherulites whose size, neatness, and regularity are quite comparable to that shown by the iPP phase crystallized

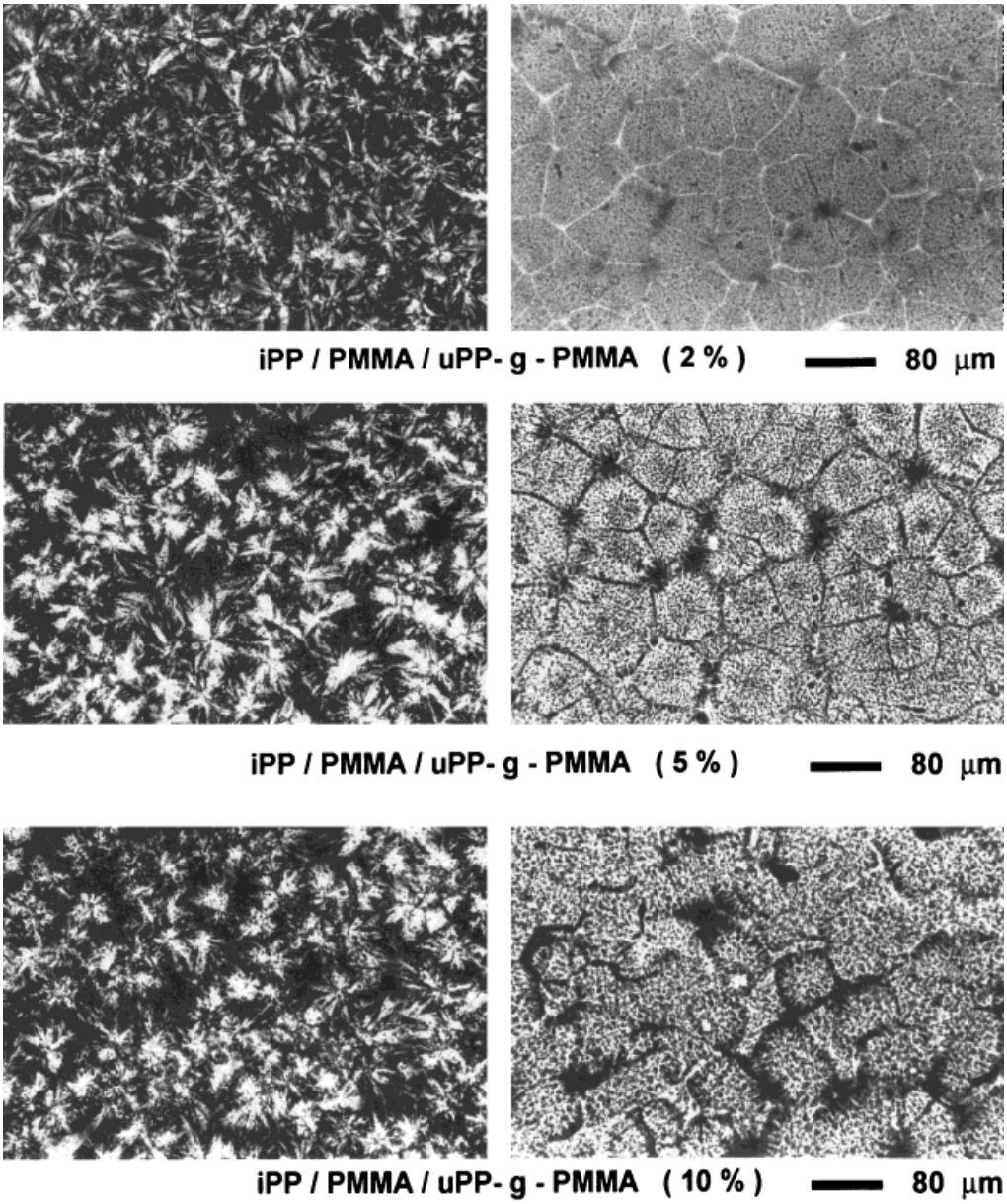

Figure 6 Optical micrographs taken with crossed and parallel polarizers of thin films of iPP/aPMMA/uPP-*g*-PMMA ternary blends containing 2, 5, and 10% (w/w) of uPP-*g*-PMMA copolymer.

from its iPP/aPMMA binary blends. With increasing uPP-*g*-PMMA content (w/w) the iPP spherulites tend to become more open and coarse; such an effect is composition dependent. Comparatively more open and coarse spherulites are in fact exhibited by the ternary blends containing the highest uPP-*g*-PMMA content (see Fig. 6). Such a morphological result suggests that the amount of uncrystallizable material located in interfibrillar and interlamellar regions of iPP crystals increases with increasing uPP-*g*-PMMA content. Moreover, for all the ternary blends investigated the examination of the thin films shows that amorphous interspherulitic contact regions are developed; such an effect is also composition dependent. Both dimensions and number per unit area of such amorphous regions tend to increase with increasing uPP-*g*-PMMA content (w/w), in-

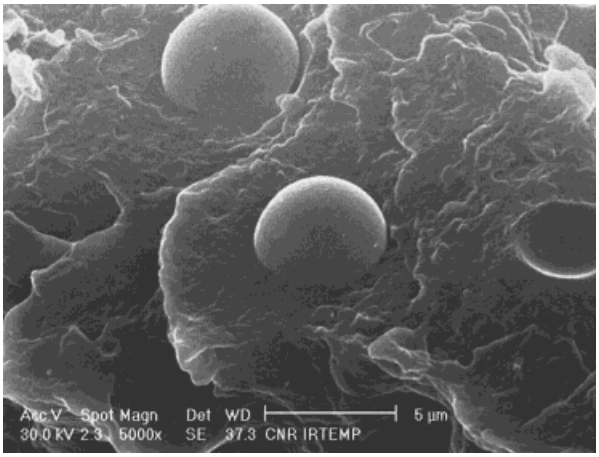

Figure 7 SEM micrographs of cryogenic fracture surfaces of iPP/aPMMA binary blends (original magnification ×5000).

dicating that the rejection phenomenon of uncrystallizable material from the iPP crystal front becomes more pronounced with increasing copolymer content. Such results could be accounted for by hypothesizing that the growth front of the iPP crystals selectively rejects the uncrystallizable molecules in interfibrillar or interspherulitic regions according to their chemical constitution and configurational regularities (i.e., the rejection undergone increases with decreasing such regularities). The possibility that the increased rejection phenomenon is related to the state of mixing of the blend components also has to be taken into account, that is, the miscibility effects in the amorphous state among propylenic sequences of the uPP-*g*-PMMA copolymer and iPP as suggested by DMTA results previously reported.

From the SEM investigations performed on cryogenically fractured surfaces of iPP/aPMMA films, the PMMA particles show a relatively narrow size distribution with diameters ranging between 1.5 and 5.0 μm. Moreover, the smooth surfaces of debonded particles and the clean holes, where the particles separated from the iPP matrix during the fracture, show poor adhesion between the phases (see Fig. 7). The uPP-*g*-PMMA addition, irrespective of blend composition, does not promote the two effects generally provided by the presence of compatibilizer at the interface in immiscible blends such as iPP/aPMMA blends. The expected effects were an increase of adhesion between the phases and a decrease of the interfacial tension between them; the smaller phase size plus increased phase adhesion results in improved mechanical properties. SEM analysis of cryogenically fractured film surfaces for all the investigated ternary blends reveals in fact that the PMMA domains show a continuous distribution function of particle size and that the size ranges of such domains, obtained by quantitative image analysis of several SEM photomicrographs, are almost constant with no dependence on uPP-*g*-PMMA content. The achievement of such a dispersion degree indicates that the extent of compatibilization is essentially the same for each PMMA based particles formed, irrespective of blend composition. Moreover, little evidence of increased interfacial adhesion or interconnection between the phases can be observed (see Figs. 8–10). From all the morphological results obtained it may be concluded that, in the iPP/aPMMA/uPP-*g*-PMMA blends, the uPP-*g*-PMMA copolymer is mainly dispersed in the iPP matrix and deeply modifies the crystalline texture of such materials.

WAXS Studies

Typical WAXS diffractograms of thin films of binary iPP/aPMMA and ternary iPP/aPMMA/uPP-*g*-PMMA blends are shown in Figures 11 and 12. All the samples give diffraction peaks whose angles are characteristic for the crystal structure of the α form of PP and in addition show a broad diffraction noncrystalline halo. Such a noncrystalline halo is centered at 2θ equal to 16.8° for the binary iPP/aPMMA blend; for the plain iPP and PMMA such a halo is centered at 2θ val-

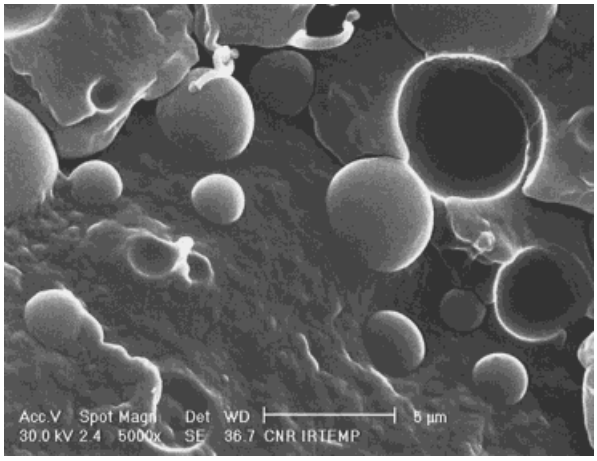

Figure 8 SEM micrographs of cryogenic fracture surfaces of iPP/aPMMA/uPP-*g*-PMMA ternary blends containing 2% (w/w) of uPP-*g*-PMMA copolymer (original magnification ×5000).

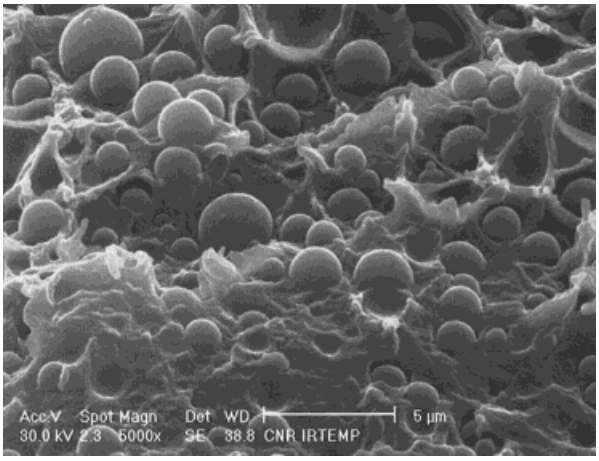

Figure 9 SEM micrographs of cryogenic fracture surfaces of iPP/aPMMA/uPP-*g*-PMMA ternary blends containing 5% (w/w) of uPP-*g*-PMMA copolymer (original magnification ×5000).

ues of 16.8° and 13.8°, respectively. By adding 2% (w/w) of uPP-*g*-PMMA copolymer the noncrystalline halo of the resulting ternary blends shifts toward a lower 2θ value (16.4°) approaching the value shown by the amorphous phase of the plain uPP-*g*-PMMA copolymer (16.2°). A further shift of such a halo toward a comparatively lower angle (15.5°) is induced by increasing the uPP-*g*-PMMA content (5% w/w); such a 2θ value remaining unaffected by adding more uPP-*g*-PMMA (10% w/w). Note that the 2θ value of 15.5° is lower than that found for the amorphous phase of the plain uPP-*g*-PMMA copolymer, suggesting that in these ternary blends the amorphous phase could have a composition different from that of both binary iPP/aPMMA blends and plain uPP-*g*-PMMA copolymer.

The apparent crystal size (D) of iPP in the perpendicular direction to the (110), (040), and (130) crystallographic planes was calculated by Sherrer equation (16):

$$D_{hkl} = \frac{K\lambda}{\beta_o \cos(\theta_{hkl})}$$

where β_o is the half-width in radians of the reflection corrected for instrumental broadening and λ is the wavelength of the radiation used (1.5418 Å). The shape factor K is set equal to unity and so the size data have to be considered as relative data. The absence in the WAXS diffractograms of (220) reflection did not allowed correction for lattice distortion of $D(110)$. The crystal size of plain iPP and uPP-*g*-PMMA copolymer together with those of the binary and ternary blends are reported in Table IV. In the direction perpendicular to the crystallographic plane (110) the apparent crystal size found for the iPP phase crystallized in the presence of PMMA is higher than that of the plain iPP. For the ternary blends the $D(110)$ values range between the values shown by the plain iPP and the iPP/aPMMA blends depending on the uPP-*g*-PMMA content (w/w). In particular, for low copolymer content the $D(110)$ value is, within experimental error, the same value has shown by the plain iPP. With increasing uPP-*g*-PMMA content such a value tends to approach that of the iPP phase crystallized from the iPP/aPMMA blends. The $D(040)$ values of the plain iPP are higher than that found for the iPP phase crystallized from both binary and ternary blends. In the direction perpendicular to the (130) crystallographic plane the crystal size of the iPP phase for the iPP/aPMMA binary blends and for the ternary blends containing low uPP-*g*-PMMA content are lower than that shown by the plain iPP. Opposite results are obtained for the ternary blends containing larger uPP-*g*-PMMA content (see Table IV). For the uPP-*g*-PMMA copolymer, no $D(130)$ value can be determined owing to the peak broadness. The higher crystal growth in the direction perpendicular to the (130) crystallographic plane of the iPP phase crystallized from the ternary blends containing, respectively, 5% (w/w) and 10% (w/w) of uPP-*g*-PMMA copolymer seems to not be related to

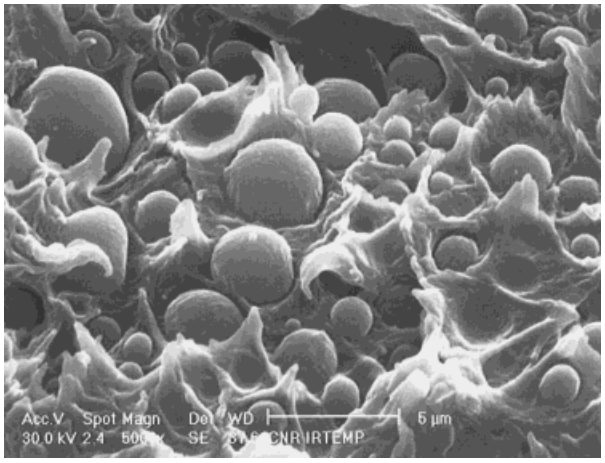

Figure 10 SEM micrographs of cryogenic fracture surfaces of iPP/aPMMA/uPP-*g*-PMMA ternary blends containing 10% (w/w) of uPP-*g*-PMMA copolymer (original magnification ×5000).

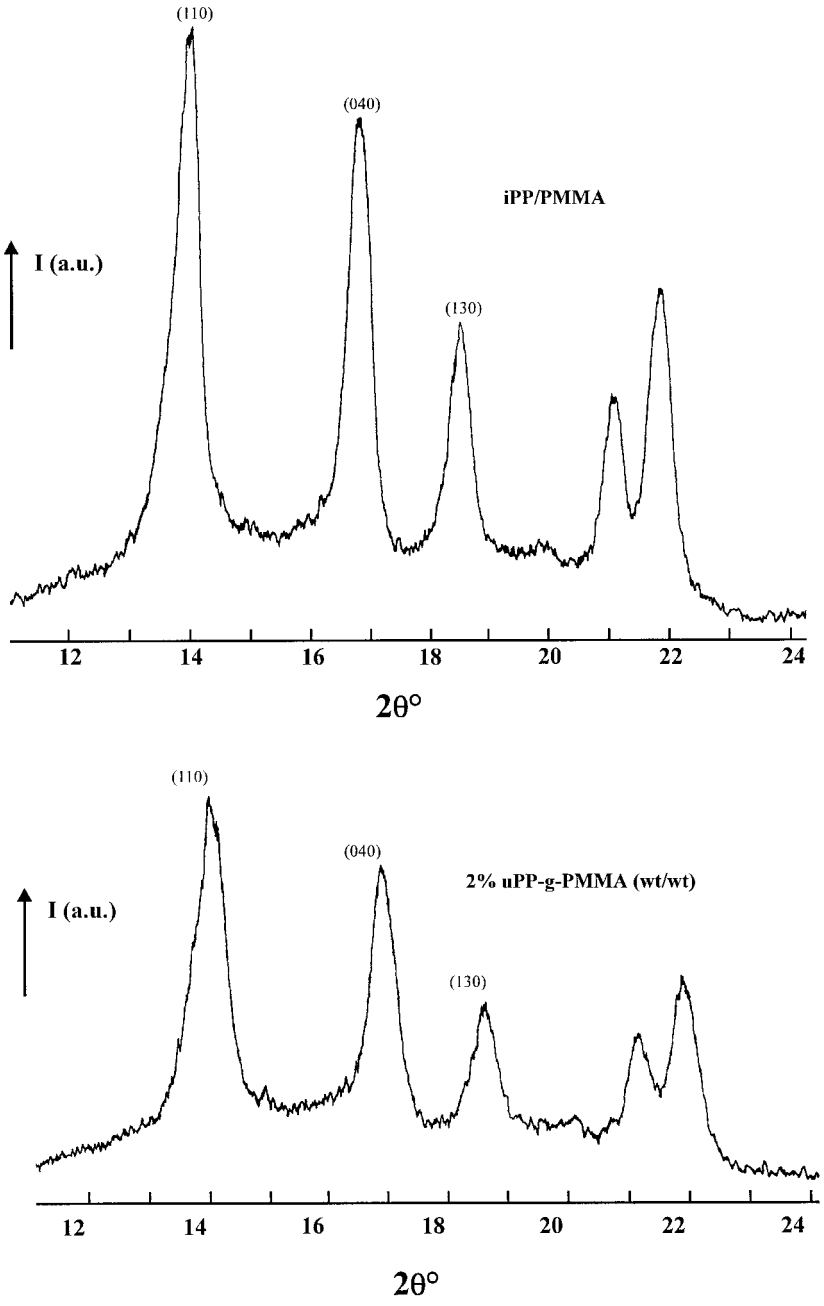

Figure 11 WAXS diffractograms of binary iPP/aPMMA blends and iPP/aPMMA/uPP-*g*-PMMA ternary blends containing 2% (w/w) of uPP-*g*-PMMA copolymer.

undercooling effects because the DSC experiments revealed that such a graft copolymer has no nucleation ability on the iPP crystallization process. It could be supposed therefore that the observed increase in the $D(130)$ values is to be ascribed to the growth of crystals from both the iPP and propylenic sequences of the uPP-*g*-PMMA copolymer.

SAXS Studies

Typical Lorentz-corrected desmeared patterns for samples of binary iPP/aPMMA and ternary iPP/aPMMA/uPP-*g*-PMMA blends are shown in Figure 13. The SAXS profiles exhibit well defined maxima; by applying Bragg's law the long period (L) of the iPP phase has been calculated from the

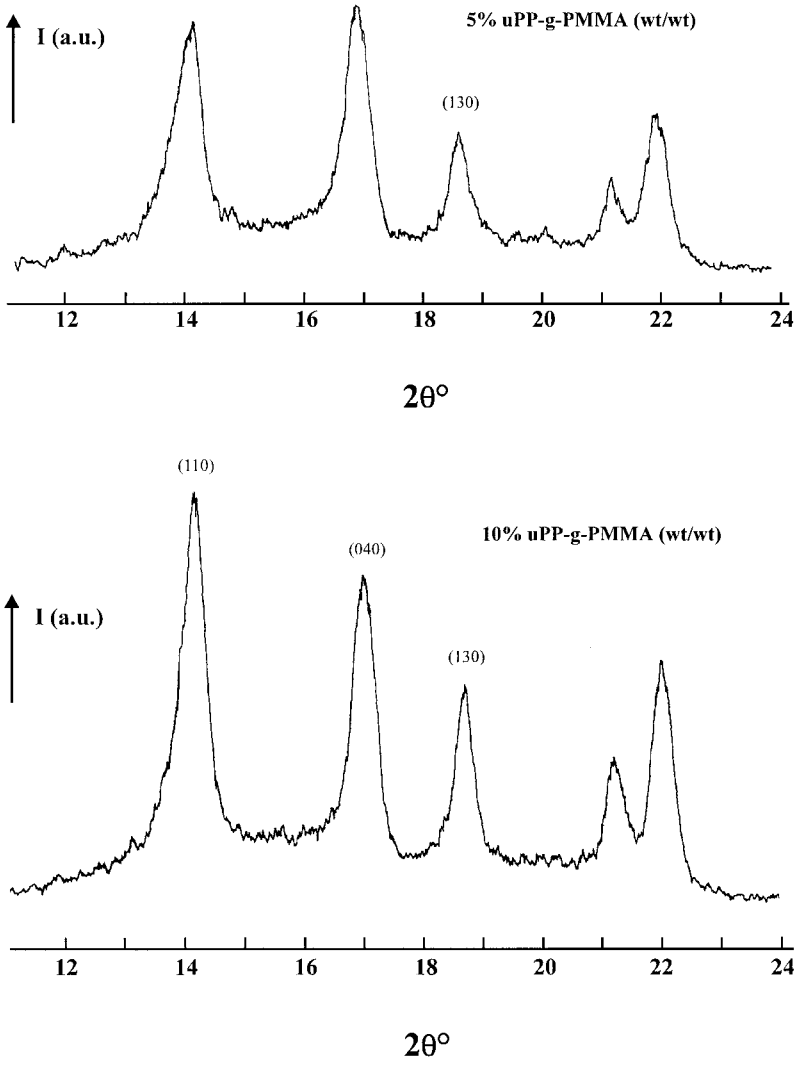

Figure 12 WAXS diffractograms of iPP/aPMMA/uPP-*g*-PMMA ternary blends containing 5 and 10% (w/w) of uPP-*g*-PMMA copolymer, respectively.

peak position. The peak position for the ternary blends shifts to comparatively lower angles and such effect is composition dependent. Assuming a two phase model for the iPP spherulite fibrillae, consisting of alternating parallel crystalline lamellae and amorphous layers, the crystalline lamellar thickness (L_c) has been calculated using the following relation for the L values:

$$L_c = \frac{X_{c\,(\mathrm{iPP})} \cdot L}{(\rho_c/\rho_a)(1 - X_{c\,(\mathrm{iPP})}) + X_{c\,(\mathrm{iPP})}}$$

where $X_{c\,(\mathrm{iPP})}$ is the DSC crystallinity index of the iPP phase and ρ_c and ρ_a are the densities of the crystalline and amorphous iPP phase, respectively.

The thickness of the amorphous interlamellar layer (L_a) has been calculated by

$$L_a = L - L_c$$

The long period, lamellar thickness, and amorphous interlamellar thickness of the plain iPP and iPP crystallized from its binary and ternary blends are reported in Table V. For the plain iPP and iPP crystallized from the iPP/aPMMA blends the L, L_c, and L_a values are within experimental error (50 nm), confirming that the iPP phase structure remains unaffected by the presence of the PMMA phase. On the other hand, for the ternary blends, L values increase markedly with increasing uPP-*g*-PMMA content (see Table V);

Table IV Apparent Crystal Size (D) of Crystals of Plain iPP and Its Binary and Ternary Blends and of Plain uPP-*g*-PMMA Copolymer in Direction Perpendicular to 110, 040, and 130 Crystallographic Planes

Sample	$D_{(110)}$ (Å)	$D_{(040)}$ (Å)	$D_{(130)}$ (Å)
iPP	74	112	128
iPP/aPMMA	94	99	119
iPP/aPMMA/uPP-*g*-PMMA graft 2% (w/w)	71	89	94
iPP/aPMMA/uPP-*g*-PMMA graft 5% (w/w)	89	99	138
iPP/aPMMA/uPP-*g*-PMMA graft 10% (w/w)	94	99	149
uPP-*g*-PMMA	52	94	—

Table V Long Period (L), Crystalline Lamella Thickness (L_c), and Interlamellar Amorphous Thickness (L_a) for Plain iPP and Its Binary and Ternary Blends and for Plain uPP-*g*-PMMA Copolymer

Sample	L (Å)	L_c (Å)	L_a (Å)
iPP	201	106	95
iPP/aPMMA	197	100	97
iPP/aPMMA/uPP-*g*-PMMA graft 2% (w/w)	216	105	111
iPP/aPMMA/uPP-*g*-PMMA graft 5% (w/w)	270	137	133
iPP/aPMMA/uPP-*g*-PMMA graft 10% (w/w)	319	150	169
uPP-*g*-PMMA	115	37	78

moreover, a plot of the L values versus the uPP-*g*-PMMA content (w/w) reveals that there is a linear dependence of the L values upon the copolymer content (w/w) (see Fig. 14). According to the model used, the surprising increase of the long period with uPP-*g*-PMMA composition is due to the increase in both the average crystalline thickness and interlamellar amorphous phase (see Table V). Thus, when iPP crystallizes in the presence of the uPP-*g*-PMMA copolymer the phase structure developed in the blends results in lamel-

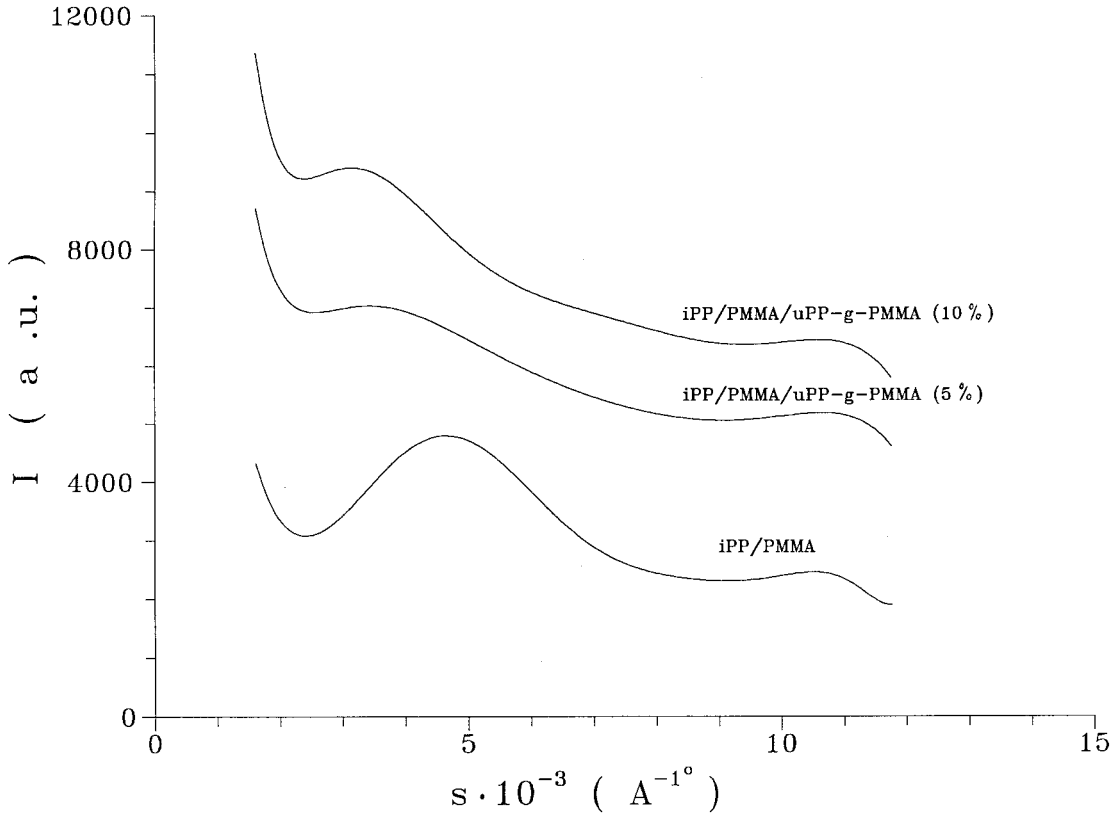

Figure 13 Typical SAXS Lorentz corrected desmeared patterns of iPP/aPMMA binary and iPP/aPMMA/uPP-*g*-PMMA ternary blends.

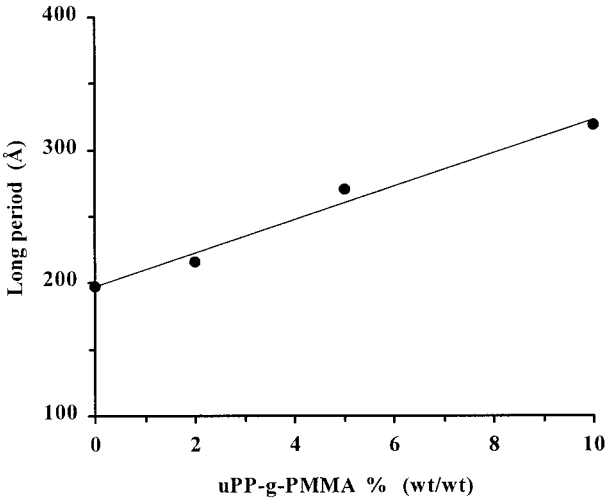

Figure 14 Plot of the long period (L) of the iPP phase as a function of uPP-*g*-PMMA copolymer content.

lar thickness and an interlamellar amorphous layer higher than those shown by plain iPP and higher with increasing uPP-*g*-PMMA content (w/w). For uPP-*g*-PMMA content up to 5% (w/w), the increase observed in L_a values is comparable to that observed in L_c values, whereas comparatively higher L_a value is shown by the iPP phase crystallized from the blends containing 10% (w/w) of the uPP-*g*-PMMA copolymer (see Fig. 14, Table V). Assuming on the basis of the evidence so far obtained that the PMMA sequences of the uPP-*g*-PMMA copolymer tend to be mainly rejected by the iPP crystallizing front in interfibrillar and/or interspherulitic amorphous contact regions, the observed increase in both L_c and L_a values of the iPP phase crystallized from its ternary blends can be accounted for by the occurrence of a cocrystallization phenomenon among propylenic sequences of uPP-*g*-PMMA copolymer and iPP. During such a process it cannot be excluded that PMMA chains characterized by comparatively lower molecular mass remain entrapped in the iPP interlamellar amorphous regions forming their own domains. Therefore, the development of the iPP lamellar structure can be modeled as a function of the copolymer content according to the schematic model reported in Figure 15. Work is in progress to assess the validity of the conclusions reached by the present SAXS analysis investigating the structure of the phases and interphases developed in binary iPP/uPP-*g*-PMMA blends. An increase in iPP L values was also found when studying phase and interphase structures generated in iPP/aPS blends by adding 2, 5, and 10% (w/w) of a graft copolymer of propylene with styrene (uPP-*g*-PS) synthesized according to the same patents used for synthesizing the uPP-*g*-PMMA copolymer.[1] It is very interesting to point out that, even though for a given blend composition the L values shown by the iPP phase crystallized from the iPP/aPMMA/uPP-*g*-PMMA give results comparable to that shown by the iPP phase crystallized from iPP/aPS/uPP-*g*-PS blends,[1] the iPP phase crystallized from iPP/aPMMA/uPP-*g*-PMMA blends is characterized by comparatively higher crystalline lamellar thickness and consequently lower amorphous interlamellar thickness. Such findings could suggest that the propylenic sequences of the uPP-*g*-PMMA copolymer are characterized by constitutional and configurational regularities, which are required for the crystallization process of iPP phase, that are higher than that of the uPP-*g*-PS copolymer.

CONCLUDING REMARKS

Blends of iPP and aPMMA exhibit a coarse domain morphology that is characteristic of immiscible blends. Using a novel graft copolymer of propylene with MMA (uPP-*g*-PMMA) as a compatibilizer for iPP/aPMMA blends, with the focus on iPP/aPMMA (80/20) composition, this study led to the conclusion that, contrary to expectation, the uPP-*g*-PMMA addition provides no compatibilized materials. The dispersion degree achieved, irrespective of uPP-*g*-PMMA content (w/w), is comparable to that developed in iPP/PMMA binary blends with no relevant evidence of increased adhesion or interconnection between the phases. On the other hand the crystalline texture of such iPP based materials has been found to be deeply modified by the uPP-*g*-PMMA presence, such an effect being composition dependent. OM investigations show in fact that with increasing uPP-*g*-PMMA content the iPP spherulites become more open and coarse, indicating the location of uncrystallizable material in the iPP interfibrillar and interlamellar regions. Moreover, an increase in dimensions and number per unit area of the amorphous interspherulitic contact regions with increasing uPP-*g*-PMMA content (w/w) occurs. Such morphological results have been explained in terms of selective rejection of uncrystallizable molecules from the growth front of the iPP crystals and/or miscibility effects among propylenic sequences of the uPP-*g*-PMMA copolymer and iPP as suggested by DMTA results. SAXS experi-

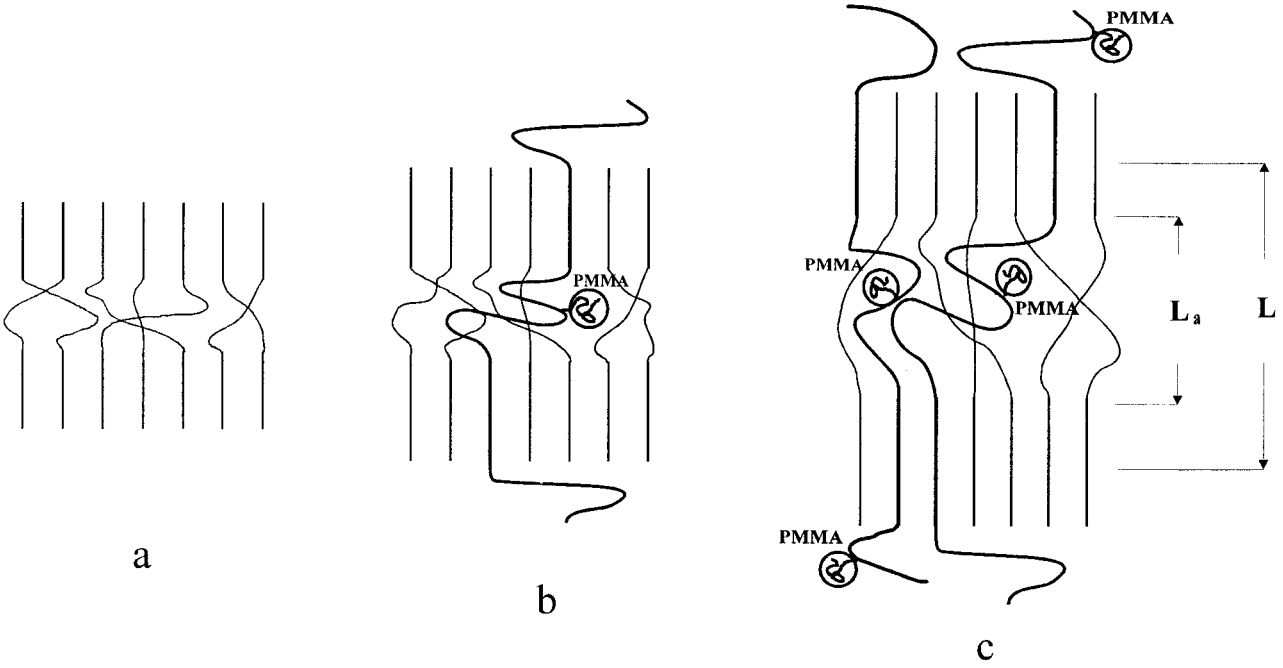

Figure 15 Schematic model of the iPP lamellar structure developed in iPP/aPMMA/uPP-*g*-PMMA blends as a function of copolymer content: (a) 0% (w/w) uPP-*g*-PMMA, (b) 5% (w/w) uPP-*g*-PMMA, and (c) 10% (w/w) uPP-*g*-PMMA.

ments demonstrate that the phase structure developed in the iPP/aPMMA/uPP-*g*-PMMA blends is characterized by long period values that increase linearly with increasing uPP-*g*-PMMA content (w/w). In particular, assuming for the iPP spherulite fibrillae a two phase model consisting of alternating parallel crystalline and amorphous layers, the crystalline lamellar thickness and the amorphous interlamellar thickness are higher than that shown by the plain iPP and are higher with higher uPP-*g*-PMMA content (w/w). Such results have been explained by the occurrence of a cocrystallization phenomenon among propylenic sequences of the uPP-*g*-PMMA copolymer and iPP. The development of the iPP lamellar structure in the iPP/aPMMA/uPP-*g*-PMMA blends has been modeled by hypothesizing that, during such a cocrystallization process, copolymer PMMA chains with comparatively lower molecular mass remain entrapped in the iPP amorphous layer forming their own domains. Evidence of a strong correlation between the crystallization process of the uPP-*g*-PMMA copolymer and the iPP crystallization process has also been clearly shown by DSC experiments. The thermograms of both solution cast and nonisothermally crystallized samples of iPP/aPMMA/uPP-*g*-PMMA blends exhibit in fact a single endothermic peak that widens with increasing copolymer content showing that the perfection and thickness of iPP crystals is noticeably affected by the uPP-*g*-PMMA presence. A comparable increase in L values by SAXS was shown by the iPP phase crystallized from iPP/aPS/uPP-*g*-PS blends, even though the L_c and L_a values have been found to be respectively lower and higher than that determined for an iPP phase crystallized from iPP/aPMMA/uPP-*g*-PMMA blends.[1] It is pointed out that the uPP-*g*-PS addition provided iPP/aPS compatibilized materials; the uPP-*g*-PS formed a coating layer around the aPS particles or interpenetrated the two homopolymers phases.[1] The very different behavior of uPP-*g*-PMMA and uPP-*g*-PS copolymers in modifying mode and state of dispersion of the minor component and phase structure of the iPP matrix is presumably related to their different graft content (w/w) and/or length and distribution of the grafted chains (i.e., to their different molecular architecture). Even though both the copolymers are characterized by a comblike structure[4] from all the results obtained by studies performed to date on iPP/aPMMA/uPP-*g*-PMMA and iPP/aPS/uPP-*g*-PS blends, it is suggested that the grafting of short chains with frequent insertion points into the backbone chain of propylene copolymer (uPP)

produces a copolymer (uPP-*g*-PS) showing a noticeable capability of selectively penetrating the corresponding homopolymeric phases (i.e., an effective compatibilizer agent for iPP based materials). The grafting of long chains with few insertion points into uPP backbone produces, on the other hand, a copolymer (uPP-*g*-PMMA) that essentially modifies the intrinsic phase structure of the iPP matrix, that is, the crystalline texture of the materials.

REFERENCES

1. L. D'Orazio, R. Guarino, C. Mancarella, and E. Martuscelli, *J. Appl. Polym. Sci.,* **65,** 1539 (1997).
2. G. Cecchin, F. Guglielmi, and F. Zerega, U.S. Pat. 4,602,077 (1986).
3. G. Cecchin and A. De Nicola, U.S. Pat. 5,159,023 (1990).
4. L. D'Orazio, C. Mancarella, E. Martuscelli, and G. Sticotti, *J. Mater. Sci.,* **30,** 4960 (1995).
5. L. D'Orazio, C. Mancarella, and E. Martuscelli, *Polymer,* **32,** 1186 (1991).
6. L. D'Orazio, C. Mancarella, E. Martuscelli, and G. Sticotti, *J. Mater. Sci.,* **26,** 4033 (1991).
7. L. D'Orazio, C. Mancarella, E. Martuscelli, and G. Sticotti, *Polymer,* **34,** 3671 (1993).
8. L. D'Orazio, C. Mancarella, E. Martuscelli, and G. Sticotti, *J. Appl. Polym. Sci.,* **53,** 387 (1994).
9. L. D'Orazio, C. Mancarella, E. Martuscelli, and G. Sticotti, *Advanced Routes for Polymer Toughening,* Elsevier, Amsterdam, (1996), Chap. 5.
10. L. D'Orazio, C. Mancarella, E. Martuscelli, and G. Sticotti, *Polymer,* to appear.
11. S. Brandrup and E. M. Immergut, *Polymer Handbook,* Vol. 5, Interscience, New York, 1975.
12. C. G. Vonk, *J. Appl. Crystallogr.,* **8,** 340 (1975).
13. L. E. Alexander, *X Ray Diffraction in Polymer Science,* Wiley, New York, 1969.